Title

Variegated clonality and rapid emergence of new molecular lesions in xenografts of acute lymphoblastic leukemia are associated with drug resistance

Journal

Experimental Hematology, 43(1)

ISSN

0301-472X

Authors

Nowak, Daniel
Liem, Natalia LM
Mossner, Maximilian
et al.

Publication Date

2015

DOI

10.1016/j.exphem.2014.09.007

Peer reviewed

HHS Public Access

Author manuscript

Exp Hematol. Author manuscript; available in PMC 2018 April 11.

Published in final edited form as:

Exp Hematol. 2015 January ; 43(1): 32–43.e1-35. doi:10.1016/j.exphem.2014.09.007.

Variegated clonality and rapid emergence of new molecular lesions in xenografts of acute lymphoblastic leukemia are associated with drug resistance

Daniel Nowak[a,b], **Natalia L.M. Liem**[c], **Maximilian Mossner**[b], **Marion Klaumünzer**[b], **Rachael A. Papa**[c], **Verena Nowak**[a,b], **Johann C. Jann**[b], **Tadayuki Akagi**[d], **Norihiko Kawamata**[a], **Ryoko Okamoto**[a], **Nils H. Thoennissen**[a], **Motohiro Kato**[e], **Masashi Sanada**[e], **Wolf-Karsten Hofmann**[b], **Seishi Ogawa**[e], **Glenn M. Marshall**[f], **Richard B. Lock**[c], and **H. Phillip Koeffler**[a,g]

[a]Division of Hematology and Oncology, Cedars Sinai Medical Center, University of California, Los Angeles, School of Medicine, Los Angeles, CA, United States

[b]Department of Hematology and Oncology, Medical Faculty Mannheim of the University of Heidelberg, Heidelberg, Germany

[c]Children's Cancer Institute Australia for Medical Research, Lowy Cancer Research Centre, University of New South Wales, Sydney, Australia

[d]Department of Stem Cell Biology, Graduate School of Medical Science, Kanazawa University, Ishikawa, Japan

[e]Department of Pathology and Tumor Biology, Graduate School of Medicine, Kyoto University, Kyoto, Japan

[f]Kids Cancer Centre, Sydney Children's Hospital, Randwick, Australia

[g]National University of Singapore, Singapore, Singapore

Abstract

The use of genome-wide copy-number analysis and massive parallel sequencing has revolutionized the understanding of the clonal architecture of pediatric acute lymphoblastic leukemia (ALL) by demonstrating that this disease is composed of highly variable clonal ancestries following the rules of Darwinian selection. The current study aimed to analyze the molecular composition of childhood ALL biopsies and patient-derived xenografts with particular emphasis on mechanisms associated with acquired chemoresistance. Genomic DNA from seven primary pediatric ALL patient samples, 29 serially passaged xenografts, and six in vivo selected chemoresistant xenografts were analyzed with 250K single-nucleotide polymorphism arrays. Copy-number analysis of non–drug-selected xenografts confirmed a highly variable molecular pattern of variegated subclones. Whereas primary patient samples from initial diagnosis displayed

Offprint requests to: Dr. Daniel Nowak, Department of Hematology and Oncology, Medical Faculty Mannheim of the University of Heidelberg, Pettenkofer Strasse 22, Mannheim 68169, Germany; daniel.nowak@medma.uni-heidelberg.de.
RBL and HPK contributed equally to this work.

Supplementary data related to this article can be found online at http://dx.doi.org/10.1016/j.exphem.2014.09.007.

Conflict of interest disclosure: No financial interest/relationships with financial interest relating to the topic of this article have been declared.

a mean of 5.7 copy-number alterations per sample, serially passaged xenografts contained a mean of 8.2 and chemoresistant xenografts a mean of 10.5 copy-number alterations per sample, respectively. Resistance to cytarabine was explained by a new homozygous deletion of the *DCK* gene, whereas methotrexate resistance was associated with monoallelic deletion of *FPGS* and mutation of the remaining allele. This study demonstrates that selecting for chemoresistance in xenografted human ALL cells can reveal novel mechanisms associated with drug resistance.

Current treatment of pediatric acute lymphoblastic leukemia (ALL) consists of empirically optimized combinations of antileukemic drugs such as glucocorticoids, vincristine (VCR), asparaginase, methotrexate (MTX), mercaptopurine, cytarabine (ARA-C), cyclophosphamide, and others [1], which achieve five-year survival rates of 80% to 90% [2]. However, deaths due to relapse, primary treatment failure, or disease progression still occur in 10% to 15% of cases [2]. The elucidation of biological mechanisms for such relapses would improve treatment outcome for pediatric ALL.

In this context, xenograft models of ALL in immunodeficient (NOD/SCID) mice have proven to be valuable tools to study this disease in vivo [3–5]. Primary ALL cells derived from patient biopsies have minimal capacity for proliferation using currently available in vitro cell culture techniques. Xenograft models allow massive cell expansion and facilitate in vivo preclinical testing of experimental therapies. Moreover, the process of serial xenotransplantation has enabled the identification and study of rare subsets of leukemia cells, which possess repopulation capacity, giving support for the tumor stem cell concept in leukemia and solid tumors [6,7].

With regard to the molecular pathogenesis of pediatric and adult ALL, substantially new understanding has been gained by the analysis of primary ALL samples with high density single-nucleotide polymorphism (SNP) arrays. Single-nucleotide polymorphism arrays allow a detailed genome-wide mapping for cryptic copy-number alterations (CNAs) and loss of heterozygosity such as copy-number neutral loss of heterozygosity (CNLOH), adding to the discovery of several important and prognostically relevant genomic lesions such as microdeletions of *IKZF1* and *PAX5* in ALL [8–12].

The combination of xenotransplantation models with high throughput genomic analysis, including SNP arrays, has recently led to the discovery that the subclonal architecture of ALL and acute myeloid leukemia cells is complex and variegated with linear or branching evolutionary histories [13–15].

In light of this, the aim of the current study was to assess the molecular composition of childhood ALL samples xenografted in immunodeficient mice with and without chemo-therapeutic drug selection pressure. We explored the possibility of using this model to determine molecular mechanisms of chemoresistance when ALL xenografts were exposed in vivo to various chemotherapeutic agents used in the standard treatment of pediatric ALL. Single-nucleotide polymorphism arrays were used to perform a genome-wide copy-number analysis to compare several parameters: (1) xenografts compared with their matched primary biopsy, (2) xenografts subjected to up to four serial passages in comparison with their primary diagnostic sample, and (3) xenografts rendered chemoresistant in vivo against single

chemotherapeutic compounds versus their passage-matched control cells. Our findings indicate that ALL continues to clonally evolve following the process of xenografting and that these cells had the capacity to quickly give rise to clones carrying molecular lesions associated with chemoresistance, which were sometimes not detectable in diagnostic samples by current methods.

Materials and methods

Development of xenografts, selection of in vivo–derived drug-resistant sublines, and study of in vivo drug responses

All experimental studies were approved by the Human Research Ethics Committee and the Animal Care and Ethics Committee of the University of New South Wales. Procedures by which xenografts from childhood ALL biopsies in immune-deficient NOD/SCID (NOD.CB17-Prkdc^{scid}/SzJ) mice were established have been described in detail previously [5,16]. Briefly, to establish initial xenografts, 2.5–10 × 10^6 mononuclear cells from bone marrow or peripheral blood biopsies were injected into the tail veins of 5- to 8-week-old female NOD/SCID mice. On the day of inoculation, mice received 250 cG of total body irradiation at a dose rate of 325 cG/min by parallel opposed 4 MV x-rays. Patient and xenograft characteristics are presented in Table 1 and have in part been described previously [16–18]. Continuous xenografts were established by inoculating 5 × 10^6 spleen-derived cells from highly engrafted mice into the tail veins of secondary recipient mice. For all mouse experiments involving patient-derived xenografts, the number of mice that successfully engrafted compared with the number inoculated exceeded 90%.

For in vivo selection of drug resistant sublines of xenografts ALL3 and ALL17, mice were treated with single agent vincristine (0.5 mg/kg weekly), cytarabine (100 mg/kg Monday through Friday every 3 weeks), methotrexate (5 mg/kg Monday through Friday every 2 weeks), or dexamethasone (DEX; 15 mg/kg Monday through Friday weekly). All drugs were administered by intraperitoneal (IP) injection. Leukemia engraftment and response to drug treatment were assessed by weekly enumeration of the proportion of human CD45$^+$ cells in the peripheral blood (%huCD45) [5]. Owing to previous experience showing that low level dissemination of xenograft cells into the peripheral blood is associated with high level infiltration of bone marrow and spleen [19], drug treatments were initiated when the %huCD45 reached 1% and continued until the %huCD45 increased through the drug treatments or until animals experienced leukemia- or drug-related morbidity. The number of emerging chemoresistant xenograft lines compared with the number of mice inoculated is depicted in Supplementary Table E1 (online only, available at www.exphem.org).

For confirmation of in vivo drug resistance, spleen-derived cells were engrafted into groups of three to four secondary recipient mice. Drug treatments were initiated when the %huCD45 reached 1% and consisted of vincristine (0.5 mg/kg IP × 4 weeks), cytarabine (100 mg/kg Monday through Friday IP every 3 weeks × 4), methotrexate (5 mg/kg Monday through Friday IP every 2 weeks × 4), or dexamethasone (15 mg/kg IP Monday through Friday weekly × 4). Individual mouse event-free survival (EFS) was calculated as the days from treatment initiation until the % huCD45 reached 25% or mice exhibited signs of leukemia-related morbidity. Event-free survival was represented graphically by Kaplan-

Meier analysis, and survival curves were compared by the log rank test. The efficacy of drug treatment was evaluated by leukemia growth delay (LGD), calculated as the difference between the median EFS of vehicle control and drug-treated cohorts.

Extraction of genomic DNA

Genomic DNA (gDNA) was isolated with the DNeasy Blood and Tissue kit (QIAGEN, Valencia, CA) either from mononuclear cells of primary pediatric ALL biopsy samples obtained at diagnosis or relapse or from spleen-derived xenograft cells at a purity of >90% huCD45^{+}. A total of $n = 42$ gDNA samples were analyzed (Tables 1 and 2).

High density single-nucleotide polymorphism array analysis

Approximately 250 ng of gDNA from each sample was processed according to the genomic mapping 250K NspI protocol and hybridized to 250K NspI SNP arrays using the GeneChip Fluidics station 450 and GeneChip Scanner 3000 (Affymetrix, Santa Clara, CA) as described previously [20,21]. Data analysis of deletions, amplifications, and CNLOH was performed using the CNAG software (Copy Number Analyzer for Affymetrix GeneChip, Cancer Genomics Projekt, University of Tokyo, Japan) with nonmatched references as previously described [20,21]. Size, position, and location of genes contained in CNAs were determined with the University of California, Santa Clara, Genome Browser (http://genome.ucsc.edu/) and the Ensemble Genome Browser (http://www.ensembl.org/index.html). We excluded CNAs involving immunoreceptor and immunoglobulin genes from analysis. Genomic copy-number polymorphisms were excluded by comparison of the detected genomic lesions with the registered copy-number polymorphisms in these genome browsers.

Validation of copy number alterations and sequencing of mutations

For confirmation of genomic copy-number changes, Sybr-green quantitative real-time polymerase chain reaction (PCR) was performed on the gDNA of an in vivo cytarabine-selected subline (ALL17-ARA-C-R) and its corresponding passage-matched control sample (ALL17-CTL1) according to the $2^{-\Delta\Delta CT}$ method [22] on a Lightcycler 480 (Roche, Mannheim, Germany). The relative allele dosage of the putatively deleted genomic region in the drug-selected sample was compared with the same region in the control sample and with the allele dosage in the genomic regions flanking the deletion in both samples. All primer sequences are available on request. Sequencing of the *FPGS* gene was performed by direct Sanger sequencing of PCR-amplified genomic DNA on a 3130 Genetic Analyzer (Applied Biosystems, Waltham, MA). Deep sequencing of the identified *FPGS* mutation was carried out in a basic amplicon sequencing setup on a 454 GS Junior System (Roche).

Results

Single-nucleotide polymorphism array analysis of serial xenograft passages reveals heterogenic patterns of genomic alterations and indicates a diverse clonal architecture in acute lymphoblastic leukemia

To investigate the influence of serial passaging on DNA CNAs, we utilized a large panel of continuous xenografts that had previously been established in NOD/SCID mice for up to four passages [5] as well as patient biopsy samples obtained at diagnosis or relapse (Tables 1

and 2). A total of seven primary pediatric ALL patient samples obtained at diagnosis or relapse, 29 untreated xenografts, and six in vivo drug-selected xenograft sublines were interrogated for acquired CNAs (Table 2). A mean of 5.7 CNAs/sample from the primary patient samples, 8.2 CNAs/sample in the untreated ALL xenografts, and 10.5 CNAs/sample in the in vivo drug-selected xenografts were identified (Table 3). Most CNAs were heterozygous and homozygous deletions, but duplications, amplifications, and CNLOHs were also present and frequently affected common target genes such as *CDKN2A/CDKN2B, PAX5*, and *ETV6*. A complete and detailed documentation of all 343 identified CNAs is contained in Supplementary Tables E2–E4 (online only, available at www.exphem.org).

In the 29 untreated xenograft samples, seven sets had been serially passaged up to four times from the original diagnosis biopsy specimen. The CNAs of these seven sets showed that the xenografts established at first passage very frequently displayed genomic alterations different from those present in the original biopsy. Furthermore, serial transplantations following establishment of the initial xenograft revealed that their CNAs also diverged in a variegated fashion. In some of the xenograft lines with changing genomic profiles, specific genomic alterations were retained in all subsequent passages, while others were gained or lost in some xenografts.

This level of complexity is highlighted in Figure 1, which provides an overview of different patterns of genomic alterations found in serial transplantations of the diagnosis sample from which xenograft ALL25 was established as well as the patient's biopsy obtained at relapse. While an unbalanced *E2A-PBX1* translocation was retained throughout all samples of this case (primary and xenografts), the cells of the first-passage xenograft harbored additional deletions of *IKZF1, PAX5*, and other regions. By contrast, the second-passage xenograft showed the identical genotype as the primary patient sample. From this, it can be hypothesized that the predominant clone detected in the first xenograft passage evolved from the predominant clone in the primary patient sample by acquisition of additional genomic deletions. However, the predominating clone in the second xenograft passage must have grown from the minor E2A-PBX1–only clone, which persisted in the first-passage xenograft. The third- and fourth-passage xenografts displayed a third clone, carrying a homozygous deletion of *CDKN2A/B* and additional deletions at other loci. It cannot be determined from these data whether this new clone was an evolved clone from the clone-engrafted second-passage xenograft or an outgrowth of a minor clone already present in the primary patient sample and then carried over in the serial transplantations. However, the data make clear that the analyzed ALL sample consists of a highly complex clonal architecture with multiple clonal populations with distinctly diverging molecular profiles. Interestingly, in this case, the only constant alteration was the unbalanced *E2A-PBX1* translocation, while other important recurrent molecular alterations typical for ALL, such as deletions of *IKZF1, PAX5*, and *CDKN2A/B*, occurred only intermittently.

As depicted for ALL25, almost all analyzed series of primary patient samples and their serially transplanted xenografts showed diverse genetic architectures. Similarly to ALL25, all cases displayed CNAs, which were retained in all samples, suggesting that these may be important driver lesions of these cells, while other lesions displayed great variability. Table 4

summarizes this observation, showing that constant lesions consisted of ALL-typical translocations, such as *E2A-PBX1* or *ETV6-RUNX1*, but also recurrent homozygous deletions of *CDKN2A/B*. Interestingly, other commonly affected genes in ALL, such as *IKZF1* and *PAX5*, were found in the variable set of lesions. Detailed CNA visualization in the sets of xenograft passages are shown in Supplementary Figures E1–E26 (online only, available at www.exphem.org).

In vivo selection of drug-resistant xenograft sublines and analysis of patterns of in vivo drug resistance

To assess the effects of in vivo selection with established chemotherapeutic drugs on DNA CNAs, drug-resistant sublines were generated by treating mice engrafted with second-passage ALL3 and ALL17 cells with single agent vincristine, cytarabine, methotrexate, or dexamethasone. Figure 2 depicts the emergence of the ALL3 and ALL17 sublines following exposure to single-agent drug treatments. The frequency with which drug-resistant lines emerged remained relatively consistent across all four drugs (mean = 41%, range = 40% to 50%; Supplementary Table E1, online only, available at www.exphem.org). However, drug-resistant sublines emerged at a markedly higher frequency for ALL17 (71%) compared with ALL3 (17%).

To confirm that the emergence of xenograft cells during in vivo drug treatments was due to the acquisition of cellular drug resistance rather than host-derived epiphenomena, spleen-derived cells from ALL3 and ALL17 drug-selected sublines were retransplanted into secondary recipient mice to test their in vivo drug responses. For each of the sublines tested, marked resistance to the selecting drug was observed (Table 5; Supplementary Figure E27; online only, available at www.exphem.org). The LGDs for vincristine and dexamethasone were approximately halved for ALL17-VCR-R1 and ALL17-DEX-R, respectively, and reduced by almost 90% for vincristine in ALL3-VCR-R, compared with their respective passage-matched control sublines. The acquisition of methotrexate resistance by ALL17-MTX-R was more profound, with an almost complete loss of in vivo drug sensitivity. Similarly, ALL17-ARA-C-R cells were profoundly resistant to cytarabine, with an approximately tenfold reduction in LGD compared with passage-matched control cells. These results confirmed that the in vivo emergence of drug-selected sublines is associated with profound levels of resistance to the selecting drug.

We next sought to determine whether the in vivo drug-selected sublines exhibited cross-resistance to established drugs used in the treatment of pediatric ALL. When treated with vincristine, cytarabine, methotrexate, or dexamethasone, the EFS of mice engrafted with ALL17-ARA-C-R, ALL17-MTX-R, and ALL17-DEX-R was not significantly different compared with passage-matched controls, indicating that resistance was only apparent to the selecting drug (Table 5).

Single-nucleotide polymorphism array analysis of in vivo drug-selected xenografts reveals genomic lesions involved in chemoresistance

To gain a greater understanding of mechanisms of chemoresistance in pediatric ALL, the in vivo drug-selected sublines were subjected to SNP array analysis and compared with their

respective passage-matched controls. A total of seven newly acquired CNAs were identified in ALL3-VCR-R, ALL17-ARA-C-R, and ALL17-MTX-R (Table 6).

The vincristine-selected ALL3-VCR-R subline displayed a newly acquired partial deletion of *CDK6* on chromosome 7q21.2 (Table 6; Supplementary Figure E28A, online only, available at www.exphem.org) and a new trisomy 18 (Table 6; Supplementary Figure E28B, online only, available at www.exphem.org). In ALL17-ARA-C-R, we observed a homozygous deletion of part of the *DCK* gene (Fig. 3A and Table 6). This deletion was detected by three SNP probe sets of the array (Fig. 3B). Fine mapping and measurement of the allelic dosage by quantitative real-time PCR of genomic DNA confirmed a homozygous deletion of exons 3 and 4 of *DCK* (Fig. 3C).

The methotrexate-resistant xenograft subline ALL17-MTX-R displayed enlargement of an already-existing heterozygous deletion on chromosome 9q encompassing over 50 genes (Fig. 4A). One gene in this newly deleted region was *FPGS*, which is directly involved in methotrexate metabolism [23]. Direct Sanger sequencing of the remaining allele of this gene revealed a newly acquired missense mutation at codon 470 (p.H470R) that was not found in the passage-matched control sample (Fig. 4B). There was no corresponding entry to this variant in the Cosmic database (http://cancer.sanger.ac.uk/cancergenome/projects/cosmic/). According to analysis with PolyPhen-2 (http://genetics.bwh.harvard.edu/pph2/), this mutation was predicted to be possibly damaging with a score of 0.551 (sensitivity: 0.88; specificity: 0.91). Interestingly, there is a registered nonsynonymous SNP in close proximity to this mutation (rs35789560, p.R466C), which has negative effects on the enzyme kinetics [24]. To elucidate whether this mutation was already present at low levels in the untreated control sample, amplicon deep sequencing of this region was performed. Despite reaching twelvethousand-fold coverage of the analyzed region, the mutation could not be detected, even at low levels, in the control sample.

Discussion

New, powerful genomic high-throughput techniques, such as genome-wide copy-number analysis using SNP arrays and massive parallel DNA sequencing techniques, allow insights into the heterogeneity of the ALL genome. It is composed, not of a linearly and sequentially developed dominant clone but of a large collection of variable subclonal populations with a complex branching architecture of ancestry as shown here and by others [14,15]. For cancer genomics and therapy, this has the wide-ranging consequence of opening a new avenue to study the specific molecular profiles of disease-founding cell clones.

Existing studies assessing the molecular profiles of ALL relapse samples in comparison with their diagnostic sample have shown that many of the lesions of the relapse clone overlap with lesions of the predominant diagnostic clone, suggesting a common founding origin, but other lesions in the relapse clones differed. In these cases, it was sometimes possible by using sensitive molecular techniques to show that such altered relapse clones were already present in low proportions at diagnosis, suggesting that relapse alterations confer resistance to treatment [1,25,26]. To address mechanisms of resistance acquisition, several strategies have been employed previously, such as whole-exome sequencing approaches of ALL

relapse samples versus their diagnosis samples, leading to the identification of activation mutations of drug-inactivating enzymes [27]. Another approach consisted of treating ALL cell lines in vivo to investigate specific pathways involved in drug-induced cell killing such as reversal of glucocorticoid resistance by Akt inhibition [28]. Artificial induction of chemoresistance in ALL cell lines xenografted into immunodeficient mice has been used to test the biological behavior of resistant lines in the setting of graft-versus-leukemia effect [29] or multidrug-resistant mechanisms under treatment with vincristine [30]. However, a targeted analysis of the molecular dynamics of primary ALL cells in vivo under active selection pressure by standard ALL treatment compounds, such as glucocorticoids, vincristine, methotrexate, or cytarabine, has not been performed to our knowledge.

By analysis with high-density SNP arrays of 29 ALL xenografts at different stages of serial transplantation and seven primary patient samples, we confirmed that the ALL xenografts in our study displayed a variegated subclonal branching architecture as shown previously [14,15]. This was evidenced by emergence and clearance of variable clones with different genomic lesions. It was interesting that some lesions, such as *E2A-PBX1* and *ETV6-RUNX1* translocations, were retained in all clones, suggesting that these may be important founder or driver lesions, while other ALL-typical genomic deletions containing *PAX5* or *IKZF1* remained variable, suggesting that these may be dispensable. Although *PAX5* and *IKZF1* could robustly be detected in larger deletions, it is possible that microdeletions of these two genes have been missed in other samples due to relatively low probe coverage on the microarrays for these regions.

Having demonstrated variegated clonal architecture in ALL xenografts, we next showed that the established xenografts could be artificially rendered chemoresistant in vivo against single drugs by repeatedly treating them with standard antileukemic drugs used in the clinic, and thereby we established a new model for studying in vivo chemoresistance. The subsequent copy-number analysis of the xenografted samples showed that there was a trend toward an increased mean number of CNAs in serially passaged xenografts compared with their matched primary patient samples. In the chemoresistant xenografts, the mean number of CNAs was even higher. However, this could also be a reflection of the subtype of the primary leukemia from which these xenografts were derived, since these biopsy samples were not available for a baseline comparison. Nevertheless, these data are in line with previous results indicating that the procedure of xenografting alone allows for the selection of aggressive subclones already present in the primary diagnostic patient sample, whose molecular profile more closely resembles relapse samples of these patients than the diagnostic sample [31]. This could be a reflection of clonal evolution to adapt to restraints associated with the new xenogeneic microenvironment.

In the data from six pairs of chemoresistant ALL xenografts versus their untreated controls, vincristine-, cytarabine-, and methotrexate-resistant samples displayed newly acquired genomic CNAs, while the dexamethasone-resistant sample did not display any new CNAs. This could perhaps be explained by the far higher genotoxicity of the other three drugs, which are all able to induce increased oxidative stress and DNA breakage [32–34] and may therefore cause an increased occurrence of the observed structural copy-number alterations and DNA breakage as compared with glucocorticoid-induced apoptosis [35]. For the case of

vincristine resistance (sample series ALL3), it is unclear how the observed newly acquired genomic changes of a partial *CDK6* deletion and trisomy 18 mediate resistance against the drug. Known mechanisms of resistance against vincristine are limited to observations of a multidrug resistance phenotype, tubulin alterations, and resistance to vincristine-induced apoptosis [36]. Interestingly, the sample pair of ALL3 did not display a genomic deletion of *CDKN2A*. Therefore, the partial deletion of *CDK6* in the vincristine-resistant sample could represent a mechanism of altering cell-cycle regulation to overcome apoptotic signaling induced by vincristine.

In the other two cases of either cytarabine or methotrexate resistance, the newly acquired mechanisms of molecular resistance were more accessible to interpretation. The cytarabine-resistant cells (xenograft ALL-17) developed a homozygous deletion of the *DCK* gene. Deoxycytidine kinase is an enzyme that catalyzes the initial step of the 5′-phosphorylation of three of the four natural deoxyribonucleosides: deoxycytidine, deoxyguanosine, and deoxy-adenosine. Deoxycytidine kinase is also an essential enzyme for the phosphorylation of cytarabine and other nucleoside analogues to their monophosphate forms [37–39]. Disruptions of the function of the *DCK* gene, such as by reduced expression of deoxycytidine kinase, have been associated with resistance to cytarabine [40–42]. To our knowledge, this is the first report of a partial homozygous deletion of *DCK* (exons 3–4) as a mechanism of cytarabine resistance.

The methotrexate-resistant xenograft (ALL17-MTX-R) displayed an enlarged deletion of the long arm of chromosome 9 in comparison to its passage-matched control xenograft. Within the newly acquired deletion is the coding region for the gene *FPGS*, which catalyzes the polyglutamylation of folates and antifolates after uptake into the cell [43,44]. This metabolism creates antifolate polyanions that can no longer be effluxed out of cells, thereby leading to enhanced intracellular retention and increased cytotoxic activity. Therefore, loss of *FPGS* activity is an established mechanism of resistance to antifolates dependent on polyglutamylation in vitro and in vivo [45,46]. Inactivating mutations of *FPGS* have been associated with resistance to antifolate therapy [47,48]. In these previously reported cases, the mutations of *FPGS* were biallelic, implying that the gene function can be rescued by a remaining intact allele if the other one is mutated. The biological effect of the acquired missense mutation H470 R in the *FPGS* gene in our study has not been proven functionally. However, it is highly likely to induce resistance to methotrexate, because neither an extended heterozygous deletion, nor the preexistence of the mutation, even by deep sequencing with greater than twelvethousandfold coverage, could be detected in the passage-matched control sample. Although anecdotal, the circumstance that this mutation could not be detected in the control sample is of special note because, ostensibly, the molecular analysis of artificially rendered chemoresistant subclones of ALL xenografts in this study tested one step further the hypothesis of complex branching clonal architecture in ALL. According to this notion, the mutation should have been detectable in a minor subclone in the diagnostic sample. However, this case emphasizes a second possibility—namely that under the additional pressure of chemotherapy, the genomic variability of ALL cells in vivo is too high even to allow for rapid emergence of new chemoresistant subclones under therapy.

In conclusion, we present a comprehensive genome-wide analysis of pediatric ALL xenografts and confirm recent findings of the complex branching subclonal architecture of ALL. Importantly, we demonstrate for the first time that the model of inducing chemoresistance in xenografted human ALL cells in immunodeficient mice is highly efficient in detecting molecular alterations that confer chemoresistance against established drugs used in the treatment of pediatric ALL. Ultimately, if expanded, this experimental paradigm could be used to catalogue recurrent molecular changes in ALL cells upon induction of chemoresistance. Knowledge of such molecular lesions would, in the future, offer the possibility to prescreen patients with relapse to establish predictive models for response to different relapse therapeutic regimens with the aim of improving clinical outcomes. Moreover, this approach should yield a large number of target genes for development of strategies to circumvent resistance to therapy.

Supplementary Material

Refer to Web version on PubMed Central for supplementary material.

Acknowledgments

Dr D. Nowak has received a research grant from the Deutsche Forschungsgemeinschaft (no. 817/1-1). Prof RB Lock received a Research Fellowship from the National Health and Medical Research Council (Australia). Prof HP Koeffler was supported by the StaR Award (Singapore) and by a National Institutes of Health grant (no. 5R01CA026038-35).

References

1. Inaba H, Greaves M, Mullighan CG. Acute lymphoblastic leukaemia. Lancet. 2013; 381:1943–1955. [PubMed: 23523389]
2. Hunger SP, Lu X, Devidas M, et al. Improved survival for children and adolescents with acute lymphoblastic leukemia between 1990 and 2005: A report from the children's oncology group. J Clin Oncol. 2012; 30:1663–1669. [PubMed: 22412151]
3. Bachmann PS, Lock RB. In vivo models of childhood leukemia for preclinical drug testing. Curr Drug Targets. 2007; 8:773–783. [PubMed: 17584033]
4. Lee EM, Bachmann PS, Lock RB. Xenograft models for the preclinical evaluation of new therapies in acute leukemia. Leuk Lymphoma. 2007; 48:659–668. [PubMed: 17454623]
5. Liem NL, Papa RA, Milross CG, et al. Characterization of childhood acute lymphoblastic leukemia xenograft models for the preclinical evaluation of new therapies. Blood. 2004; 103:3905–3914. [PubMed: 14764536]
6. Bonnet D, Dick JE. Human acute myeloid leukemia is organized as a hierarchy that originates from a primitive hematopoietic cell. Nat Med. 1997; 3:730–737. [PubMed: 9212098]
7. Lapidot T, Sirard C, Vormoor J, et al. A cell initiating human acute myeloid leukaemia after transplantation into SCID mice. Nature. 1994; 367:645–648. [PubMed: 7509044]
8. Kawamata N, Ogawa S, Zimmermann M, et al. Molecular allelokaryo-typing of pediatric acute lymphoblastic leukemias by high-resolution single nucleotide polymorphism oligonucleotide genomic microarray. Blood. 2008; 111:776–784. [PubMed: 17890455]
9. Mullighan CG, Goorha S, Radtke I, et al. Genome-wide analysis of genetic alterations in acute lymphoblastic leukaemia. Nature. 2007; 446:758–764. [PubMed: 17344859]
10. Mullighan CG, Miller CB, Radtke I, et al. BCR-ABL1 lymphoblastic leukaemia is characterized by the deletion of Ikaros. Nature. 2008; 453:110–114. [PubMed: 18408710]
11. Mullighan CG, Su X, Zhang J, et al. Deletion of IKZF1 and prognosis in acute lymphoblastic leukemia. N Engl J Med. 2009; 360:470–480. [PubMed: 19129520]

12. Okamoto R, Ogawa S, Nowak D, et al. Genomic profiling of adult acute lymphoblastic leukemia by single nucleotide polymorphism oligonucleotide microarray and comparison to pediatric acute lymphoblastic leukemia. Haematologica. 2010; 95:1481–1488. [PubMed: 20435627]
13. Shlush LI, Zandi S, Mitchell A, et al. Identification of pre-leukaemic haematopoietic stem cells in acute leukaemia. Nature. 2014; 506:328–333. [PubMed: 24522528]
14. Anderson K, Lutz C, van Delft FW, et al. Genetic variegation of clonal architecture and propagating cells in leukaemia. Nature. 2011; 469:356–361. [PubMed: 21160474]
15. Notta F, Mullighan CG, Wang JC, et al. Evolution of human BCR-ABL1 lymphoblastic leukaemia-initiating cells. Nature. 2011; 469:362–367. [PubMed: 21248843]
16. Lock RB, Liem N, Farnsworth ML, et al. The nonobese diabetic/severe combined immunodeficient (NOD/SCID) mouse model of childhood acute lymphoblastic leukemia reveals intrinsic differences in biologic characteristics at diagnosis and relapse. Blood. 2002; 99:4100–4108. [PubMed: 12010813]
17. Bachmann PS, Gorman R, Papa RA, et al. Divergent mechanisms of glucocorticoid resistance in experimental models of pediatric acute lymphoblastic leukemia. Cancer Res. 2007; 67:4482–4490. [PubMed: 17483364]
18. High LM, Szymanska B, Wilczynska-Kalak U, et al. The Bcl-2 homology domain 3 mimetic ABT-737 targets the apoptotic machinery in acute lymphoblastic leukemia resulting in synergistic in vitro and in vivo interactions with established drugs. Mol Pharmacol. 2010; 77:483–494. [PubMed: 20038611]
19. Szymanska B, Wilczynska-Kalak U, Kang MH, et al. Pharmacokinetic modeling of an induction regimen for in vivo combined testing of novel drugs against pediatric acute lymphoblastic leukemia xenografts. PLoS One. 2012; 7:e33894. [PubMed: 22479469]
20. Nannya Y, Sanada M, Nakazaki K, et al. A robust algorithm for copy number detection using high-density oligonucleotide single nucleotide polymorphism genotyping arrays. Cancer Res. 2005; 65:6071–6079. [PubMed: 16024607]
21. Yamamoto G, Nannya Y, Kato M, et al. Highly sensitive method for genomewide detection of allelic composition in nonpaired, primary tumor specimens by use of affymetrix single-nucleotide-polymorphism genotyping microarrays. Am J Hum Genet. 2007; 81:114–126. [PubMed: 17564968]
22. Livak KJ, Schmittgen TD. Analysis of relative gene expression data using real-time quantitative PCR and the 2(-Delta Delta C(T)) method. Methods. 2001; 25:402–408. [PubMed: 11846609]
23. Synold TW, Willits EM, Barredo JC. Role of folylpolygutamate synthetase (FPGS) in antifolate chemotherapy; a biochemical and clinical update. Leuk Lymphoma. 1996; 21:9–15. [PubMed: 8907263]
24. Leil TA, Endo C, Adjei AA, et al. Identification and characterization of genetic variation in the folylpolyglutamate synthase gene. Cancer Res. 2007; 67:8772–8782. [PubMed: 17875718]
25. Mullighan CG, Phillips LA, Su X, et al. Genomic analysis of the clonal origins of relapsed acute lymphoblastic leukemia. Science. 2008; 322:1377–1380. [PubMed: 19039135]
26. Yang JJ, Bhojwani D, Yang W, et al. Genome-wide copy number profiling reveals molecular evolution from diagnosis to relapse in childhood acute lymphoblastic leukemia. Blood. 2008; 112:4178–4183. [PubMed: 18768390]
27. Tzoneva G, Perez-Garcia A, Carpenter Z, et al. Activating mutations in the NT5C2 nucleotidase gene drive chemotherapy resistance in relapsed ALL. Nat Med. 2013; 19:368–371. [PubMed: 23377281]
28. Piovan E, Yu J, Tosello V, et al. Direct reversal of glucocorticoid resistance by AKT inhibition in acute lymphoblastic leukemia. Cancer Cell. 2013; 24:766–776. [PubMed: 24291004]
29. Jansson J, Hsu YC, Kuzin II, Campbell A, Mullen CA. Acute lymphoblastic leukemia cells that survive combination chemotherapy in vivo remain sensitive to allogeneic immune effects. Leuk Res. 2011; 35:800–807. [PubMed: 21074852]
30. Zunino SJ, Storms DH, Ducore JM. Novel in vivo model of inducible multi-drug resistance in acute lymphoblastic leukemia with chromosomal translocation t(4;11). Cancer lett. 2010; 296:49–54. [PubMed: 20381955]

31. Clappier E, Gerby B, Sigaux F, et al. Clonal selection in xenografted human T cell acute lymphoblastic leukemia recapitulates gain of malignancy at relapse. J Exp Med. 2011; 208:653–661. [PubMed: 21464223]
32. Grant S. Ara-C: Cellular and molecular pharmacology. Adv Cancer Res. 1998; 72:197–233. [PubMed: 9338077]
33. Jiang W, Lu Y, Chen Z, et al. Studying the genotoxicity of vincristine on human lymphocytes using comet assay, micronucleus assay and TCR gene mutation test in vitro. Toxicology. 2008; 252:113–117. [PubMed: 18722497]
34. Martin SA, McCarthy A, Barber LJ, et al. Methotrexate induces oxidative DNA damage and is selectively lethal to tumour cells with defects in the DNA mismatch repair gene MSH2. EMBO Molecular Medicine. 2009; 1:323–337. [PubMed: 20049736]
35. Schlossmacher G, Stevens A, White A. Glucocorticoid receptor-mediated apoptosis: Mechanisms of resistance in cancer cells. J Endocrinol. 2011; 211:17–25. [PubMed: 21602312]
36. Gidding CE, Kellie SJ, Kamps WA, de Graaf SS. Vincristine revisited. Crit Rev Oncol Hematol. 1999; 29:267–287. [PubMed: 10226730]
37. Bouffard DY, Laliberte J, Momparler RL. Kinetic studies on 2′,2′-difluorodeoxycytidine (Gemcitabine) with purified human deoxycytidine kinase and cytidine deaminase. Biochem Pharmacol. 1993; 45:1857–1861. [PubMed: 8494545]
38. Carson DA, Wasson DB, Kaye J, et al. Deoxycytidine kinase-mediated toxicity of deoxyadenosine analogs toward malignant human lymphoblasts in vitro and toward murine L1210 leukemia in vivo. Proc Natl Acad Sci U S A. 1980; 77:6865–6869. [PubMed: 6256765]
39. Fernandez-Calotti P, Jordheim LP, Giordano M, Dumontet C, Galmarini CM. Substrate cycles and drug resistance to 1-beta-D-arabinofura-nosylcytosine (araC). Leuk Lymphoma. 2005; 46:335–346. [PubMed: 15621823]
40. Kanno S, Hiura T, Ohtake T, et al. Characterization of resistance to cytosine arabinoside (Ara-C) in NALM-6 human B leukemia cells. Clin Chim Acta. 2007; 377:144–149. [PubMed: 17097625]
41. Sarkar M, Han T, Damaraju V, Carpenter P, Cass CE, Agarwal RP. Cytosine arabinoside affects multiple cellular factors and induces drug resistance in human lymphoid cells. Biochem Pharmacol. 2005; 70:426–432. [PubMed: 15950950]
42. Song JH, Kim SH, Kweon SH, Lee TH, Kim HJ, Kim TS. Defective expression of deoxycytidine kinase in cytarabine-resistant acute myeloid leukemia cells. Int J Oncol. 2009; 34:1165–1171. [PubMed: 19287976]
43. McGuire JJ, Hsieh P, Coward JK, Bertino JR. Enzymatic synthesis of folylpolyglutamates. Characterization of the reaction and its products. J Biol Chem. 1980; 255:5776–5788. [PubMed: 6892914]
44. Poser RG, Sirotnak FM, Chello PL. Differential synthesis of methotrexate polyglutamates in normal proliferative and neoplastic mouse tissues in vivo. Cancer Res. 1981; 41:4441–4446. [PubMed: 6171339]
45. Liani E, Rothem L, Bunni MA, Smith CA, Jansen G, Assaraf YG. Loss of folylpolygamma-glutamate synthetase activity is a dominant mechanism of resistance to polyglutamylation-dependent novel antifolates in multiple human leukemia sublines. Int J Cancer. 2003; 103:587–599. [PubMed: 12494465]
46. Stark M, Wichman C, Avivi I, Assaraf YG. Aberrant splicing of folylpolyglutamate synthetase as a novel mechanism of antifolate resistance in leukemia. Blood. 2009; 113:4362–4369. [PubMed: 19131550]
47. Leclerc GJ, York TA, Hsieh-Kinser T, Barredo JC. Molecular basis for decreased folylpolygamma-glutamate synthetase expression in a methotrexate resistant CCRF-CEM mutant cell line. Leuk Res. 2007; 31:293–299. [PubMed: 16884772]
48. Zhao R, Titus S, Gao F, Moran RG, Goldman ID. Molecular analysis of murine leukemia cell lines resistant to 5, 10-dideazatetrahydrofolate identifies several amino acids critical to the function of folylpolyglutamate synthetase. J Biol Chem. 2000; 275:26599–26606. [PubMed: 10856298]

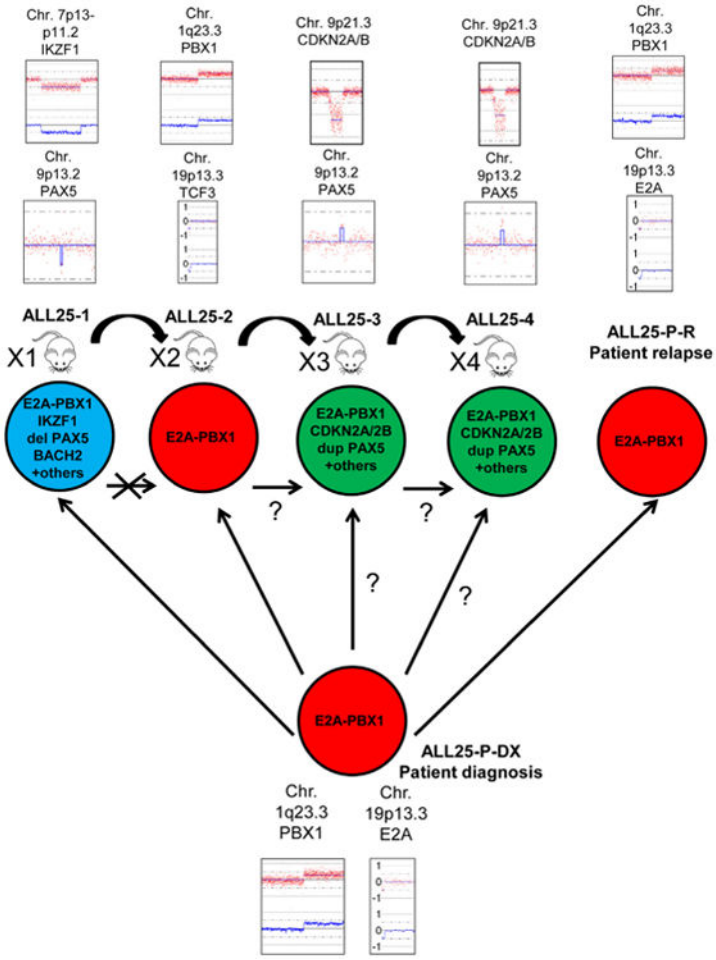

Figure 1.

Heterogeneous clonal composition of serial ALL xenografts detected by SNP array genotyping. Boxes contain views from SNP array copy-number analysis of primary ALL patient samples from initial diagnosis (ALL25-P-DX), relapse (ALL25-P-R), and four serial ALL xenograft passages of ALL25 (ALL25-1–4). The copy number is visualized by red dots, which represent one SNP each (top of each box). The blue line represents a smoothed signal of copy number. In the diploid human genome, normal copy number = 2. Downward deviation of the copy-number signal indicates either a heterozygous or homozygous deletion; upward deviation indicates either duplication or amplification. An unbalanced t(1,19) translocation (*E2A-PBX1* fusion product) is present in all samples—patient and xenograft samples. Other genomic alterations are variable and allow the inference of different subclones. Red circle: predominating clone in the primary patient sample containing an unbalanced *E2A-PBX1* translocation. This clone is also found in the second-passage xenograft and the primary sample from relapse. Blue circle: predominating clone in xenograft passage 1. Apart from the unbalanced *E2A-PBX1* translocation, this clone contains additional lesions, such as deletions of *IKZF1, PAX5*, and *BACH2*, which could have evolved from the earlier (red) clone. Finding the red clone in xenograft passage 2 must mean that this clone persisted as a minor subclone in xenograft passage 1 and cannot have evolved from the predominating clone of that passage (crossed arrow). Green circle:

predominating clone in xenograft passages 3 and 4, which contain additional lesions in the form of *CDKN2A/B* deletions and a duplication of *PAX5*.

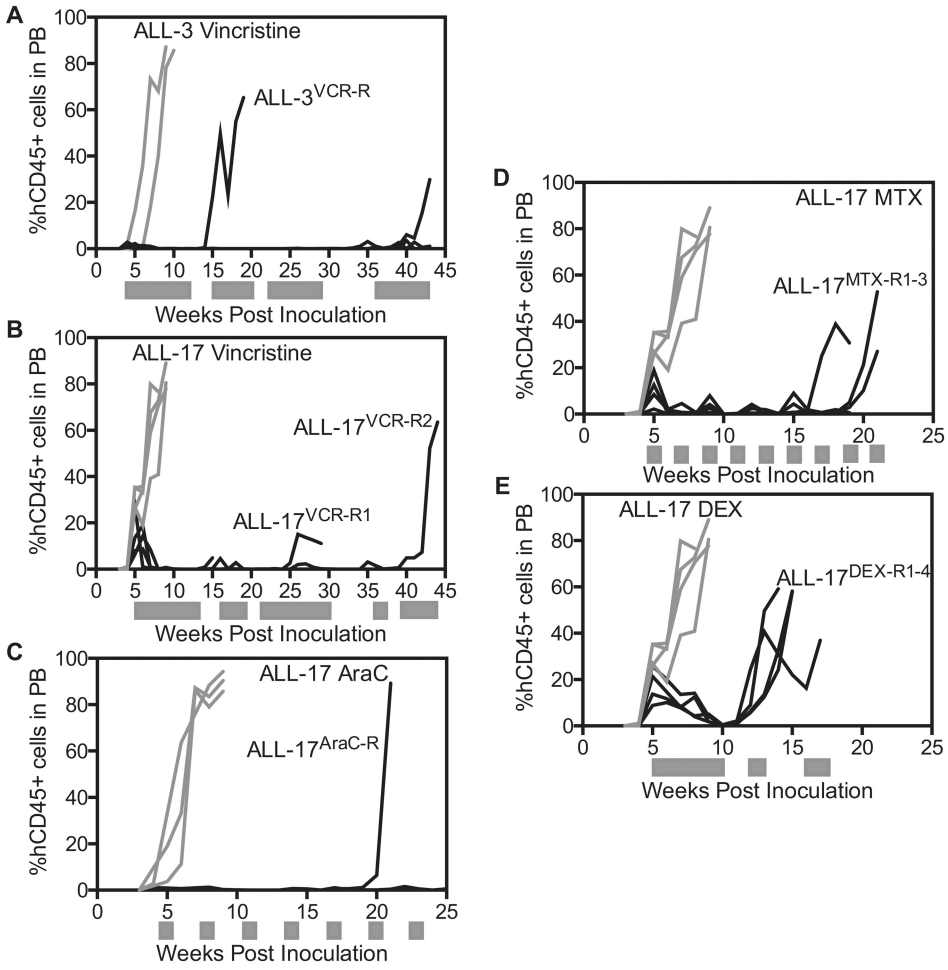

Figure 2.

In vivo selection of drug-resistant xenograft sublines. Mice were inoculated with (**A**) second-passage ALL3 or (**B–E**) ALL17 xenograft cells and monitored for engraftment by weekly tail-vein bleeds. When the percentage of cells positive for human CD45 (%huCD45) reached 1%, treatments were initiated with vincristine, cytarabine, methotrexate, or dexamethasone, as detailed in Materials and methods. Mice were culled and spleen-derived cells harvested for subsequent analysis when the %huCD45 increased through the drug treatments or when animals experienced leukemia- or drug-related morbidity. Gray bars indicate drug treatment periods. Gray lines indicate passage-matched control mice; black lines indicate drug-treated mice.

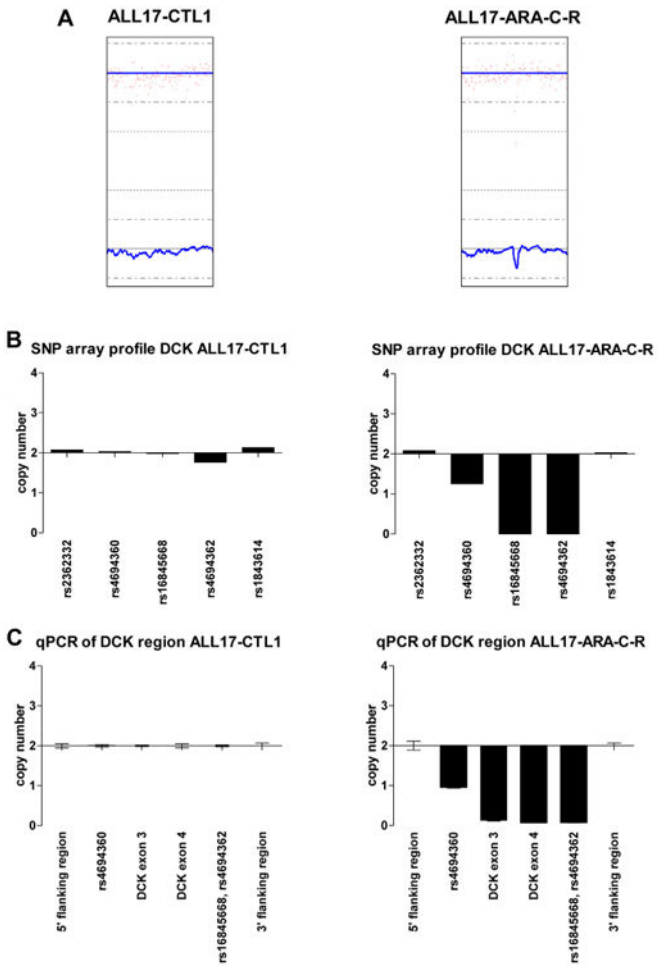

Figure 3.

Newly acquired deletion of *DCK* upon in vivo induction of chemoresistance against ARA-C in an ALL xenograft. (**A**) Magnified visualization of copy-number analysis by SNP array of part of chromosome 4q in an untreated ALL xenograft (ALL17-CTL1) and its Ara-C–resistant subclone (ALL17-ARA-C-R) with a new partial homozygous deletion of *DCK*. (**B**) The detection of the deletion is only covered by 3 SNPs on the array, which is why the absolute intensity values of these three SNPs were depicted in separate graphs. These show that, as compared with the untreated ALL control sample (left), *DCK* is heterozygously deleted in the region of the SNP rs4694360 (copy number 5 1) and homozygously deleted in the region of the SNPs rs16845668 and rs4694362 (copy number = 0). (**C**) Deletion was validated by quantitative real-time PCR of this region in the untreated sample (left) and the ARA-C resistant sample (right). *AraC* = Cytarabine.

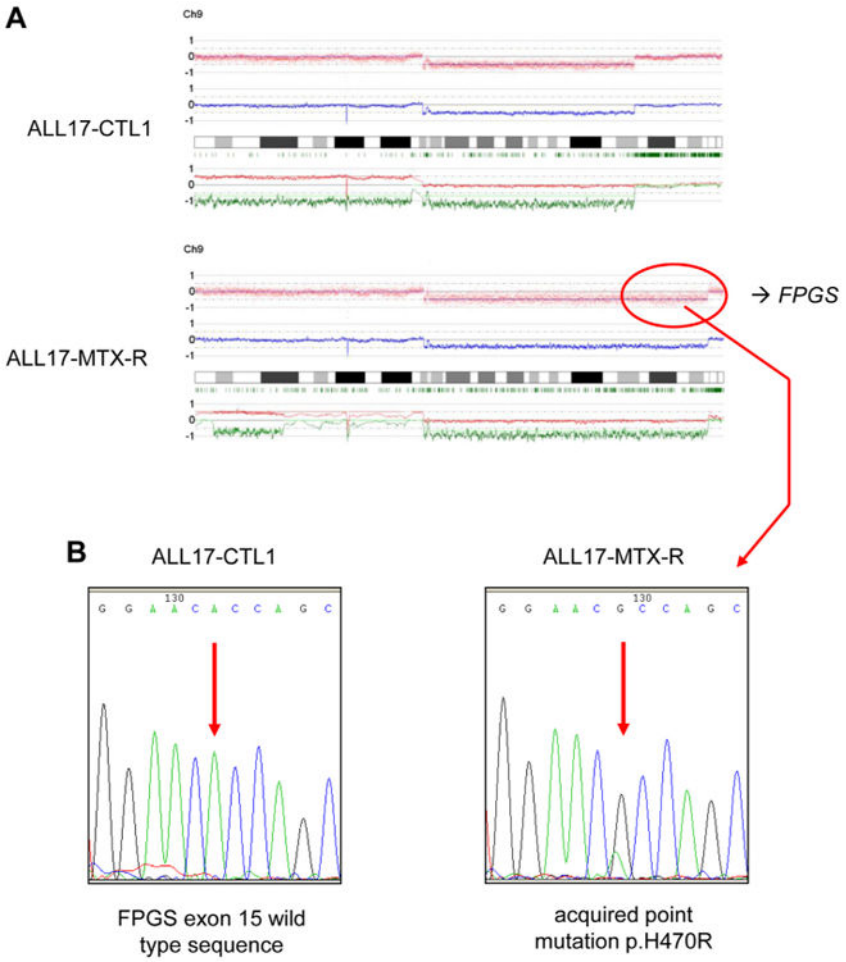

Figure 4.

Newly acquired deletion of *FPGS* upon in vivo induction of chemoresistance against MTX in an ALL xenograft. (**A**) Visualization of copy-number analysis by SNP array of chromosome 9 in an untreated ALL xenograft (ALL17-CTL1) and its MTX-resistant subclone (ALL17-MTX-R) with a new telomeric extended heterozygous deletion of the long arm of chromosome 9. (**B**) Sequencing of *FPGS* revealed a newly acquired missense mutation in the remaining allele of *FPGS* in codon 470, putatively leading to a loss of function in the remaining allele of *FPGS*.

Table 1

Patient/xenograft demographics

Patient/xenograft ID	ALL subtype	Age at diagnosis (months)	Sex	Disease status at biopsy	Risk category	WBC at biopsy (× 10^9/L)	ANZCCSG study	Cytogenetics of original patient biopsy [Number of analyzed metaphases]
ALL3	Pre-B	154	F	Diagnosis	High	93.9	6	46,XX,del(11q23)
ALL17	Common	107	F	Diagnosis	High	97.3	7	46,XX,-20, +21[18]/47,XX,-20,+21, +mar[4]
ALL25	Common	149	M	Diagnosis	Standard	4.54	8	46,XY,t(1;19)(q23;p13)
ALL26	Common	43	F	Diagnosis	Standard	90.0	8	46,XX,t(12;21)(p12;q22)
ALL27	T-ALL	104	M	Diagnosis	High	526	8	46,XY
ALL28	Common	20	M	Diagnosis	High	15.0	8	Hyperdiploid
ALL29	T-ALL	59	M	Diagnosis	High	86.3	7	46,XY
ALL30	T-ALL	90	M	Diagnosis	Very High	886	8	46,XY
ALL31	T-ALL	123	M	Diagnosis	Very High	212	8	46,XY,del(6)(q21),del(11) (q23)[4]/46, XY[14]

ANZCCSG = Australia and New Zealand Children's Cancer Study Group; *Common* = $CD10^+$ pre-B ALL; *pre-B* = B-cell precursor ALL; *T-ALL* = T-line-age ALL; *WBC* = white blood cell count.

Table 2

Experimental design and samples (*n* = 42) for analysis of genomic DNA with Affymetrix 250K arrays

	Xenografts				
Diagnosis biopsy	**Passage 1**	**Passage 2**	**Passage 3**	**Passage 4**	**Relapse biopsy**
ALL25-P-DX	ALL25-1	ALL25-2	ALL25-3	ALL25-4	ALL25-P-R
ALL26-P-DX	na	ALL26-2	ALL26-3	ALL26-4	na
ALL27-P-DX	ALL27-1	ALL27-2	ALL27-3	ALL27-4	na
ALL28-P-DX	ALL28-1	na	ALL28-3	na	na
ALL29-P-DX	ALL29-1	ALL29-2	ALL29-3	ALL29-4	na
ALL30-P-DX	ALL30-1	ALL30-2	ALL30-3	ALL30-4	na
na	ALL31a-1	ALL31a-2	ALL31a-3	ALL31a-4	na
	Passage-matched control xenografts			In vivo drug-selected xenografts	
	ALL3-CTL			ALL3-VCR-R	
	ALL17-CTL1			ALL17-VCR-R1	
	ALL17-CTL2			ALL17-VCR-R2	
	ALL17-CTL3			ALL17-ARA-C-R	
				ALL17-MTX-R	
				ALL17-DEX-R	

na = Not available.

Table 3

Frequency of CNAs detected in the ALL samples from primary patient samples in comparison with xenografts and chemoresistant xenografts

	Primary patient samples (*n* = 7)		Xenografts (*n* = 29)		Chemoresistant xenografts (*n* = 6)	
Alterations	***n***	**Mean per sample**	***n***	**Mean per sample**	***n***	**Mean per sample**
Deletions	26	3.7	170	5.9	36	6
Duplications/Amplifications	12	1.7	52	1.8	17	2.8
CNLOH	3	0.4	17	0.6	10	1.7
Total	41	**5.7**	239	**8.2**	63	**10.5**

Total mean values of CNAs are marked bold.

Table 4
Summary of constant and variable CNAs in serial xenotransplants

Series	Constant CNAs	Variable CNAs
ALL25	unbalanced *E2A-PBX1* translocation	deletions of *IKZF1, CDKN2A/B, BACH2*, and others
ALL26	unbalanced *ETV6-RUNX1* translocation	deletions of *BTG1, CEP135, ZCCHC7*, and others; UPD Chr.12p
ALL27	homozygous deletion of *CDKN2A/B*, del5q35	dup2q, del3q, del4p, del5p, del8p, deletion of *IKZF1*, del10q, del17p, and others
ALL28	hyperdiploid	none
ALL29	homozygous deletion of *CDKN2A/B*	deletion of *ETV6*, del3q13.11, dup6p, dup8p22, and dup13q14.2
ALL30	deletion of *PTEN*	duplication of *IKZF1*, dup7p21.3, and others
ALL31a	homozygous deletion of *CDKN2A/B*	dup4p12 and del9q

Del = deletion; *dup* = duplication; *UPD* = uniparental disomy.

Table 5

Median EFS and LGD of ALL17 and ALL3 sublines following in vivo exposure to VCR, ARA-C, MTX, and DEX

	EFS (days post treatment initiation)					LGD (days)			
Xenograft	**Saline**	**VCR**	**ARA-C**	**MTX**	**DEX**	**VCR**	**ARA-C**	**MTX**	**DEX**
ALL17-CTL1	11.0(11.5,11.0,8.6)	51.8 (57.2,51.8,50.9)	102 (74.7,102,108)	54.9 (53.2,54.9,58.0)	25.9 (24.7,25.9,27.0)	40.8	91.0	43.9	14.9
ALL17-VCR-R1	15.2(14.7,15.2,15.9)	**30.5** * (30.3,28.3,31.9,30.7)	>70.0(>70,>70,>70)	62.8 (49.0,62.8,62.9)	18.6 (17.4,18.6,19.9)	**15.3**	>54.8	47.6	3.4
ALL17-ARA-C-R	7.9 (4.7,11.0)	51.7 (51.2,51.7,53.1)	**21.8** * (17.7,21.8,23.7)	58.4 (56.4,60.3)	22.2(11.4,32.9)	43.8	**13.9**	50.5	14.3
ALL17-MTX-R	9.7 (7.8,9.7,11.3)	53.5 (48.7,53.5,57.9)	93.5 (93.1,93.7,98.4)	**9.2** * (9.1,9.2,19.5)	28.9 (28.3,28.9,28.9)	43.8	83.8	**−0.5**	19.2
ALL17-DEX-R	3.7 (2.4,4.9)	44.8 (41.9,44.8,52.3)	78.8 (77,80.5)	52.2 (44.8,59.6)	**10.4** * (3.2,10.4,10.5)	41.1	75.1	48.5	**6.7**
ALL3-CTL	5.3 (5.3,5.3,5.7)	75.6 (73.5,75.6,84.0)	nd	nd	nd	70.3	nd	nd	nd
ALL3-VCR-R	14.2 (7.7,14.2,19.2)	**22.8** * (20.9,22.8,23.0)	nd	nd	nd	**8.6**	nd	nd	nd

ALL17 = ALL17 xenograft; *ALL3* = ALL3 xenograft; *CTL* = untreated control; *nd* = not done; *R* = resistant.

Numbers in the EFS fields denote the median EFS, and the values below the median indicate the values of the performed experimental replicates for each condition. Median EFS values, which were significantly different from the passage-matched controls, and their corresponding LGD values are highlighted in bold.

* $p < 0.05$ compared with passage-matched control in log rank test.

Table 6

List of acquired genomic alterations in chemoresistant ALL samples in comparison with their untreated ALL controls

Sample ID	Chr. region	Start position	End position	CN	Length [Mb]	Candidate genes
ALL3-VCR-R	7q21.2	92155688	92308281	1	0.15	*CDK6*
ALL3-VCR-R	Trisomy 18			3		
ALL17-ARA-C-R	4q13.3	72229564	72258899	0	0.03	*DCK*
ALL17-ARA-C-R	20p13	2026823	2245790	3	0.22	2 genes, *STK35, TGM3*
ALL17-ARA-C-R	20p11.21	24662340	24840013	3	0.18	no genes
ALL17-ARA-C-R	20p11.21-20q11.21	24562188	29338325	CNLOH	4.78	20 genes, *ENTPD6*
ALL17-MTX-R	9q31.3-34.11	111124599	130016358	1	18.89	*FPGS*

Chr. = chromosomal; *CN* = copy number; *Mb* = mega–base pair; *R* = resistant.